Science of the Total Environment 947 (2024) 174683

Contents lists available at ScienceDirect

Science of the Total Environment

journal homepage: www.elsevier.com/locate/scitotenv

Temporal dynamics of contaminants in an estuarine system affected by acid mine drainage discharges

Evgenia-Maria Papaslioti [a], Manolis Giampouras [a], Laura Sánchez-López [a], María Dolores Basallote [b], Rémi Freydier [c], Carlos Ruiz Cánovas [a], Rafael Pérez-López [a,*]

[a] Department of Earth Sciences & Research Center on Natural Resources, Health and the Environment, University of Huelva, Campus "El Carmen", E-21071 Huelva, Spain
[b] Department of Ecology and Coastal Management, Institute of Marine Sciences of Andalusia (ICMAN-CSIC), 11510 Puerto Real, Spain
[c] HydroSciences Montpellier, Université de Montpellier, CNRS, IRD, Montpellier, France

HIGHLIGHTS

- The estuary of Huelva constitutes an extreme case of AMD contamination worldwide.
- Seasonal variations affect the neutralization of acidic rivers via seawater mixing.
- When mixing, Fe and Al precipitate as schwertmannite and basaluminite, respectively.
- Partitioning of As, Cu and Pb in the particulate phase increases by adsorption.
- Metals including Zn, Cd, Mn, Co and Ni remain mostly mobilized through mixing.

GRAPHICAL ABSTRACT

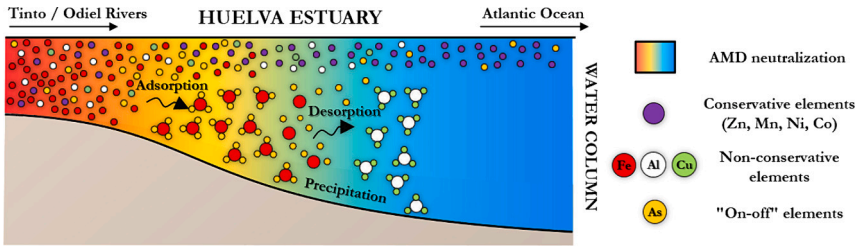

ARTICLE INFO

Editor: JV Cruz

Keywords:
Acid mine drainage
Huelva Estuary
Seawater mixing
Sorption processes
Seasonal variations
Contaminants mobility

ABSTRACT

The estuary of Huelva is constituted by the common mouth of the Odiel and Tinto rivers, which are extreme cases of acid mine drainage contamination due to the Iberian Pyrite Belt, the world's largest sulfide mineral province. The drained acidic waters are subjected to seawater mixing and thus, to dilution and precipitation processes that drive the load of contaminants entering the oceanic environment. This research reports the distribution of major metal(loid)s present in the highly acidic waters across the entire Tinto and Odiel estuarine systems as they are subjected to acid mine drainage neutralization, until reaching the ocean. The datasets presented are divided in low- and high-flow periods, corresponding to dry/warm and wet/cold seasons, respectively. Iron and Al were almost entirely removed from solution with pH increase at both periods due to their precipitation as schwertmannite and basaluminite, respectively. These mineral phases also, controlled the behavior of As, Cu and Pb, which were removed from solution, with >90 % of their concentration ending up in the particulate phase due to sorption processes. However, at pH >7, As returned entirely to the dissolved phase at both sampled seasons because of desorption, similarly to Cu at the low-flow period. On the other hand, concentrations of Zn, Cd, Mn, Co and Ni in solution decreased only by dilution with seawater, with null partitioning to any sorption processes during estuarine mixing until reaching the Atlantic Ocean.

* Corresponding author.
E-mail address: rafael.perez@dgeo.uhu.es (R. Pérez-López).

https://doi.org/10.1016/j.scitotenv.2024.174683
Received 8 April 2024; Received in revised form 8 July 2024; Accepted 8 July 2024
Available online 9 July 2024

1. Introduction

Coastal systems act as transition zones between freshwater and seawater, thus being responsible for the mass flux of contaminants that enter to deep oceanic environments. The coasts are most often influenced by estuarine environments dominated by diurnal alternations in salinity, ionic composition, and redox conditions, in accordance with the tidal and hydrological cycles, and the temporal variations (Liang and Wong, 2003). The net flux of the estuarine pollutants to the ocean depends on the fluvial inputs and their geochemical behavior (Hierro et al., 2014). For instance, estuaries trap trace elements through their sorption to particulate matter, because of solid/water interactions that lead to their net sedimentation (Bewers and Yeats, 1989). On the other hand, mineral dissolution, desorption or transformation, and resuspension of bed sediments, can also influence the migration and fate of contaminants to the open ocean (Zhou et al., 2003). Consequently, major and trace elements present in estuarine environments are characterized by either conservative or non-conservative behavior, depending on whether their concentrations are controlled only by dilution via seawater mixing or, additionally, by complex geochemical processes.

Estuarine systems represent zones of intense human occupation, so despite metals are naturally ubiquitous in aquatic systems, they are increasingly present as a result of mining and industrial activities (de Souza Machado et al., 2016). As such, they often pose a serious environmental threat, resulting in metal(loid) inputs from river catchments that eventually discharge significant loads of contaminants into the open ocean (de Souza Machado et al., 2016). Acid Mine Drainage (AMD) is a form of such water pollution associated with mining of coal or sulfide ore deposits, being an issue of global environmental concern, and responsible for the contamination and degradation of groundwaters, streams, and entire river basins (Achterberg et al., 2003; Nieto et al., 2007). While sulfides are stable and insoluble in reducing conditions, they are oxidized by chemical and microbial processes once they are exposed to atmospheric and weathering conditions by mining. As such, they generate acidity, and releasing sulfate, Fe and other metal(loid)s, depending on the host rock geology. However, it is common that AMD is neutralized by in-stream processes in large catchments. Metal behavior in AMD affected estuaries is controlled by strong pH and salinity variations, while the present particulate matter is mainly characterized by Fe oxyhydroxides, which govern the natural attenuation of trace elements by sorption processes (Achterberg et al., 2003).

The estuarine-coastal system of Huelva in SW Spain represents an extreme case of AMD pollution via the Tinto and Odiel rivers, which drain a metalliferous mining area in the Iberian Pyrite Belt (IPB), located in the SW of the Iberian Peninsula. The IPB is rich in massive metal sulfide deposits which have been exploited since 3000 BCE for the extraction of mainly gold, silver and copper (Nocete et al., 2005). Despite the level of mining activity is greatly reduced at present, the residues of past exploitations have left a large quantity of mine tailings from which metal-rich acidic discharges and eroded material are washed into the rivers (Braungardt et al., 2003; Espana et al., 2005; Cánovas et al., 2007; Nieto et al., 2013). The Tinto and Odiel rivers flow into the Atlantic Ocean forming an estuary known as Ría de Huelva (Fig. 1), contributing significant quantities of dissolved metal(loid)s (Fe, Al, As, Mn, Cu, Zn, Cd, Pb) to Gulf of Cadiz, and eventually to the deep oceanic environment (Van Geen et al., 1997; Braungardt et al., 2003). AMD-associated pollution arrival to estuarine systems has been scarcely reported, most of them referring to small streams near to the coast (e.g. Mayes and Jarvis, 2016; Chalkley et al., 2019). The anomaly of the Huelva estuary relies on the intense AMD pollution of Tinto and Odiel rivers and the lack of neutralizing materials in host rocks. As a consequence of the semiarid Mediterranean climate in the area, the metal loadings delivered to the estuary are strongly controlled by short but intense periods of rainfalls, leading to flood events, when most part of the annual flow, acidity and metal loads are carried to the estuary (Cánovas et al., 2010).

Fig. 1. A) General location map of the study area and, B) zoomed version of the study area, showing sampling points along the Tinto and Odiel Estuaries for all the sampling campaigns.

Although the extreme Tinto and Odiel rivers pollution level has been widely studied, there is a limitation in the understanding of the evolution of the physicochemical parameters and contaminants' distribution along the estuaries of both rivers to the littoral waters. In addition, the metal partitioning between dissolved and particulate matter phases across the estuary upon different rivers hydrological conditions is still understudied. In this context, the main objective of the present research is to provide insights on the spatial and seasonal variation of the Tinto and Odiel estuarine systems, covering the entire mixing zone of the rivers with seawater. For that purpose, a novel, and detailed chemical characterization was performed along both estuaries corresponding to events of both high- and low-flow of the estuarine waters based on rainy or dry periods, respectively. Although previous studies have reported the evolution of some contaminants in Tinto and Odiel estuaries separately, there is an evident lack of literature reporting the driving geochemical processes at both estuaries at the same periods, covering a wide area from the acidic river waters to the confluence of the two rivers until they reach the coastal area. Moreover, a full database on elemental concentrations in the particulate matter, additionally to the dissolved fractions, is given for the first time in those systems in different seasonal periods along both Tinto and Odiel estuaries. This novelty allows us to follow the geochemical processes that control the sorption and dissolution of the contaminants of interest, which eventually add up to the total contamination of the Atlantic Ocean.

2. Materials and methods

2.1. Study area

Most of the Tinto and Odiel rivers basins run through the IPB, which belongs to the South Portuguese Zone of the Hercynian Iberian Massif, formed by upper Palaeozoic materials containing giant and supergiant volcanogenic massive sulfide deposits (Espana et al., 2005). The principal mineral in these deposits is Pyrite (FeS_2), with lower quantities of sphalerite (ZnS), galena (PbS), chalcopyrite ($CuFeS_2$), and arsenopyrite (AsFeS), among others. The relative absence of carbonate rocks is

characteristic in the Tinto and Odiel river basins, limiting any acid-neutralizing processes that usually occur in AMD contaminated areas.

Tinto and Odiel rivers flow into a common estuary, known as the Ría de Huelva (Fig. 1), which is a dynamic system with a semidiurnal and mesotidal range (ca. 2.1 m), whose influence controls the mixing processes between highly acidic waters with alkaline seawater. The estuary is well mixed during spring tides and partially stratified during neap tides (Achterberg et al., 2003). The seasonal variations of the area owing to the Mediterranean climate, control the fluvial discharge into the estuary, varying between wet and cold periods during winter and warm and dry periods during summer (Hierro et al., 2014). As such, the average inflow of both rivers is affected accordingly with around 50 mm^3/month during wet periods and <5 mm^3/month during the driest ones (Grande et al., 2003). The fluvial waters from the drainage basins mix with the seawater following the salinity increase towards the sea, leading to an acidity neutralization process (Carro et al., 2011).

In addition, the area is affected by a large contaminant load due to the industrial activity in the adjacent areas, such as oil refineries, paper mill, fertilizer factories, sulphuric acid production facilities and a Cu smelting factory (Pérez-López et al., 2011). Among those, the activity of the phosphate fertilizer industry has produced a huge waste facility of phosphogypsum disposed directly on the salt marshes associated with the right margin of Tinto river. As such, highly acidic and contaminated leachates are discharged to the estuarine environment until nowadays, adding significantly to the contamination of the estuary of Huelva (Pérez-López et al., 2016; Papaslioti et al., 2018a; Guerrero et al., 2021). Thus, the studied system has been world-famous as one of the most heavy-metal contaminated estuaries in the world (Sainz et al., 2004), despite the fact that it contains one of the most important marsh ecosystems in Europe, the Marismas del Odiel Protected Area, declared as a Biosphere Reserve by UNESCO in 1983.

2.2. Sampling

Three sampling campaigns were performed in 2018 according to different events varying by weather conditions, along the Tinto and Odiel estuaries: i) in March during a wet period after rainy events, ii) in May during a dry period before summer, and iii) in November during a post-summer dry period. Dry periods represent low-flow river discharge (1.2 and 1.3 m^3/s for the Tinto River and 1.5 and 1.6 m^3/s for the Odiel), while the wet period corresponds to high-flow river waters after rainy events (15 and 17 m^3/s in the Odiel and Tinto rivers during November sampling, with peaks of 600 m^3/s for the Odiel the prior week). Water samples were collected at Tinto and Odiel rivers before estuarine mixing (Fig. 1; Gibraleon (GBL), Niebla (NBL), Puerto San Juan (PSJ)), along the estuarine mixing zones (TR1–8 and O1–14 samples), and after their confluence in a common estuarine channel until reaching the sea (C1–8 samples). Any observed distinct and/or additional sampling locations among sampling campaigns, are attributed to the variations in estuarine waters dynamics due to different weather conditions. Owing to the strong pH gradient (and metal concentration range), two set of sampling materials were employed to avoid cross contamination.

All materials were previously cleaned with 10 % diluted solutions of HNO_3 and afterwards, washed with distilled water. Data on pH, electrical conductivity (EC), oxidation-reduction potential (ORP) and temperature were measured in situ with a Crison MM40+ portable multiparameter instrument. A calibration at three points was performed for both EC and pH (147 μS/cm, 1413 μS/cm, and 12.88 mS/cm and 4.01, 7.00, and 9.21, respectively), while ORP was controlled using two different standard solutions (220 and 470 mV). Aliquots of all the collected samples were taken and filtered immediately on board through 0.45 μm Millipore filters fitted on Sartorius polycarbonate filter holders, for chemical analysis of the dissolved fraction. After filtration, filters were preserved to study the mineralogy of suspended material retained in the filters. Raw samples (not filtered, but acidified) were also, collected to determine the metal particulate content, being the difference between the filtered and unfiltered samples assumed to be associated with the particulate matter. Therefore, the addition of acid (HNO_3) to the unfiltered samples may dissolve the minerals (except silicates) contained in the particulate matter. The dissolved minerals include those that control the sorption of the contaminants of interest in the study area, being Fe and Al associated mineral phases. All samples and their respective physicochemical parameters are listed in Tables 1, 2, S1, S2, S3, and S4.

2.3. Analytical methods

Water samples (filtered and unfiltered) for cations and metal analysis were acidified to pH <2 with suprapur HNO_3 (2 %) and stored in the dark at 4 °C in polyethylene bottles until analysis. Acidification of the unfiltered samples served also, for the dissolution of the newly formed phases associated with acid mine drainage, as detailed in Section 2.2. Samples collected for Fe speciation and anion determinations were filtered but not acidified. Fe speciation was performed directly to the water samples by complexing with Fe(II), adding 0.5 % (*w*/w) 1,10-phenanthroline chloride solution after buffering to pH 4.5 with an ammonium acetate/acetic buffer (Rodier et al., 1996). Major elements concentrations were determined by Inductively Coupled Plasma-Atomic Emission Spectroscopy (ICP-AES; Jobin Yvon Ultima 2) at the University of Huelva. Trace elements concentrations in the different water samples from the estuary were determined by Inductively Coupled Plasma-Mass Spectrometry (ICP-MS) with a Thermo Scientific iCAP TQ ICP-MS a the "Plateforme AETE-ISO" (OSU OREME, University of Montpellier) without any prior dilution using Kinetic energy Discrimination - Argon Gas Dilution (KED-AGD mode). For trace element determinations, an internal solution containing Be, Sc, Ge, Rh and Ir was added on-line to the samples to correct signal drifts. Estuarine water and seawater reference materials for trace metals (SLEW-3 and CASS-6) were also analyzed to check the analytical accuracy, which was within 10 % of the certified values. Detection limits were between 0.02 and 0.2 mg/L for major elements and ranged from 0.23 μg/L (Zn) to 3.44 pg/L (La) for trace elements. In addition, the anions (i.e., Cl^-, Br^-, F^-, NO_3^- and NO_2^-) were determined using ion chromatography (Dionex DX-120) at the R + D laboratories of the University of Huelva, and the total alkalinity was determined by CHEMetrics® Total Titrets®, with a range of 10–100 or 100–1000 mg/L as $CaCO_3$ equivalents.

2.4. Solid phase characterization

The particulate matter accumulated in the filters was mineralogically characterized by different techniques. X-ray diffraction (XRD) patterns were obtained with a Bruker D8 Advance X-ray diffractometer with Cu Kα radiation. Diffractometer parameters were 20 mA, 40 kV and a step size of 2° 2θ/min, 3–65°. Analysis of diffraction patterns was performed with the XPowder software (Martín-Ramos, 2004). Samples were also examined by scanning electron microscopy (SEM) to obtain semi-quantitative chemical analyses and imaging of samples by an environmental scanning electron microscope coupled with a dispersive energy detector (ESEM-EDS; FEI, QEMSCAN 650F).

2.5. Geochemical modelling

Speciation-solution and reaction calculations were performed using the geochemical modelling PHREEQC-3.0 code (Parkhurst and Appelo, 2013) and the LLNL thermodynamic database (Johnson et al., 2000). This database was enlarged with data from Bigham et al. (1994) to account for schwertmannite solubility. For geochemical modelling, values of ORP were corrected to obtain Eh values, referenced to the standard hydrogen electrode (Nordstrom and Wilde, 1998). PHREEQC code was used to calculate aqueous speciation of solutions and saturation indices of the solid phases [SI = log (IAP / KS), where SI is the saturation index, IAP is the ion activity product and KS is the solid solubility product].

Table 1
Physicochemical parameters and chemical composition (concentrations in mg/L) of the dissolved phase of the samples corresponding to the low-flow period (May 2018). Elements with an asterisk (*) are given in μg/L.

Sample	pH	EC (mS/cm)	ORP (mV)	T (°C)	Fl^-	Cl^-	Br^-	SO_4^{2-}	Ca	K	Na	Si	Fe	Al	Li	B	Mn	Co*	Ni*	Cu	Zn	As*	Sr	Cd*	Ba	Pb*
PSJ	2.77	2.21	513	22.5	0.984	0.277	4.846	1036	50	7.3	120	7.5	19.31	25.10	0.083	0.354	5.194	298.1	67.43	7.626	11.52	2.201	0.424	49.01	0.034	<d.l.
TR8	2.85	2.77	502	22.9	1.204	0.440	5.938	1097	50	9.3	169	7.5	17.86	24.46	0.082	0.310	4.943	278.9	63.38	7.212	10.46	2.310	0.441	44.78	0.116	<d.l.
TR7	2.88	3.43	509	22.4	1.465	0.555	5.809	1235	62	13	235	8.2	24.78	27.93	0.105	0.362	5.967	333.4	78.89	8.536	12.73	2.398	0.575	56.67	0.032	<d.l.
TR6	2.90	3.85	508	22.0	1.762	0.715	10.02	1519	66	15	266	8.7	34.03	30.28	0.121	0.416	7.219	400.8	94.62	10.14	15.26	3.114	0.713	66.61	0.142	<d.l.
TR6-5	3.30	9.11	489	21.7	2.157	2.279	14.39	2143	91	42	1136	8.4	63.00	44.21	0.169	1.008	9.419	575.7	114.4	15.20	22.07	6.659	1.635	96.99	0.030	0.141
TR5	2.92	18.8	514	21.7	3.864	5.800	34.12	2752	134	116	2868	6.6	49.28	42.57	0.216	2.259	8.520	554.4	103.0	14.71	21.00	5.501	3.666	96.32	0.033	0.201
TR5-4	2.76	29.3	516	21.6	5.889	9.044	47.77	3025	180	181	4325	4.9	23.49	30.00	0.250	3.319	6.676	426.3	81.68	11.49	15.99	3.293	5.793	77.12	0.041	0.390
TR4	4.07	38.4	394	21.8	8.637	14.93	70.31	2934	246	275	6516	2.5	2.459	10.98	0.162	2.711	2.041	128.5	26.20	3.151	3.925	1.602	5.006	22.18	0.023	0.399
TR3	7.05	52.6	239	21.4	6.505	19.17	88.42	3086	303	395	9032	0.44	0.013	<d.l.	0.169	3.708	0.534	31.35	8.271	0.186	0.684	5.147	6.771	7.140	0.018	0.873
TR2	7.22	53.3	216	21.5	7.151	20.19	93.82	3271	309	405	9026	0.26	0.005	<d.l.	0.175	3.900	0.407	22.88	6.591	0.111	0.443	7.336	7.014	5.851	0.017	0.795
TR1	7.62	56.6	164	21.2	7.414	21.82	109.2	4179	337	390	9810	<d.l.	0.007	<d.l.	0.184	4.214	0.115	5.811	3.325	0.027	0.090	6.318	7.662	2.106	0.014	0.637
O14	3.95	8.6	421	22.0	5.455	2.266	<d.l.	1557	78	44	1110	8.6	1.586	30.15	0.126	1.565	8.853	281.2	148.4	4.721	10.70	2.568	1.407	43.92	0.047	0.253
O12	4.21	11.3	349	21.9	7.109	3.606	<d.l.	1520	93	61	1572	7.8	1.015	25.00	0.131	1.264	7.814	239.9	126.8	3.943	9.158	2.336	1.733	37.88	0.048	0.220
OX12	4.53	22.5	264	21.4	6.193	7.987	38.20	1830	150	142	3377	5.3	0.341	12.41	0.105	1.541	3.902	115.8	61.11	1.765	3.740	1.511	2.647	17.91	0.034	0.320
O10	5.53	36.7	256	21.0	5.489	13.05	60.14	2442	236	243	6237	2.1	0.073	1.057	0.177	3.813	2.719	78.82	46.49	0.994	3.016	1.219	6.159	15.64	0.050	0.655
O9	6.20	41.7	266	20.9	5.607	14.90	68.09	2730	266	267	6988	1.3	0.006	<d.l.	0.132	2.906	1.392	40.69	23.94	0.382	1.249	0.986	5.318	8.384	0.031	0.606
O8	7.51	53.7	183	21.5	7.204	20.18	89.06	3078	315	409	10,181	0.18	0.005	0.143	0.165	3.848	0.273	8.861	5.740	0.032	0.194	3.454	7.256	3.260	0.019	0.664
O2	n.a.d.	55.4	n.a.d.	n.a.d	6.572	20.65	91.71	3161	306	420	10,213	0.1	0.003	0.214	0.172	4.069	0.217	7.794	4.484	0.027	0.147	4.557	7.367	2.781	0.018	0.672
O1	7.65	57.0	169	21.1	7.355	21.55	97.59	3291	324	435	10,592	<d.l.	0.008	<d.l.	0.188	4.363	0.121	5.627	2.805	0.024	0.087	5.723	7.901	2.090	0.014	0.597
C8	7.76	57.5	181	21.1	9.120	21.88	109.7	4214	322	441	10,444	<d.l.	0.002	<d.l.	0.188	4.345	0.056	3.284	1.869	0.020	0.052	5.143	7.864	1.403	0.012	0.523
C7	7.68	57.6	186	21.3	8.061	21.70	101.2	3417	322	420	10,649	<d.l.	0.006	0.138	0.185	4.352	0.078	4.142	2.917	0.022	0.064	5.335	7.915	1.617	0.013	0.605
C5	7.81	59.4	160	20.2	5.556	22.23	99.55	3366	319	451	10,834	<d.l.	0.004	<d.l.	0.193	4.500	0.024	1.596	1.325	0.013	0.030	4.084	8.014	0.742	0.010	0.366
C4	7.73	58.5	157	19.7	5.617	22.50	97.80	3374	331	455	10,791	<d.l.	0.007	0.163	0.195	4.418	0.013	0.963	1.049	0.010	0.021	3.625	7.979	0.493	0.009	0.310
C3	7.99	59.8	151	19.4	6.607	21.46	92.97	3163	329	460	10,971	<d.l.	0.003	<d.l.	0.192	4.370	0.012	0.744	0.934	0.008	0.017	2.834	8.080	0.352	0.009	0.295
C2	7.98	60.1	179	19.5	7.028	22.44	96.70	3327	327	458	11,035	<d.l.	0.005	<d.l.	0.201	4.494	0.011	0.687	0.781	0.008	0.016	2.886	8.161	0.348	0.008	0.285
C1	7.99	60.3	176	20.2	6.912	22.75	96.69	3378	333	460	10,979	<d.l.	0.004	<d.l.	0.202	4.538	0.006	0.118	0.476	0.002	0.005	1.636	8.163	0.034	0.007	0.233

n.a.d. non available data.
d.l. detection limit.

Table 2
Physicochemical parameters and chemical composition (concentrations in mg/L) of the dissolved phase of the samples corresponding to the high-flow period (March 2018). Elements with an asterisk (*) are given in μg/L.

Sample	pH	EC (mS/cm)	ORP (mV)	T (°C)	Fl^-	Cl^-	Br^-	SO_4^{2-}	Ca	K	Na	Si	Fe	Al	Li	B	Mn	Co*	Ni*	Cu	Zn	As*	Sr	Cd*	Ba	Pb*
NBL	2.52	1.31	484	13.2	n.a.d.	n.a.d.	n.a.d.	n.a.d.	20	1.1	13	5.05	64.99	33.57	0.033	0.008	1.963	218.4	31.84	5.792	5.925	9.244	0.067	25.02	0.008	77.81
PSJ	3.89	0.83	354	19.0	0.227	0.039	0.533	278	28	2.8	48	5.9	3.085	10.30	0.019	<d.l.	1.071	68.62	15.37	1.931	1.668	0.467	0.112	10.53	0.013	59.52
TR8	3.95	0.68	449	12.9	0.270	0.069	0.624	264	25	2.1	30	5.2	0.798	7.418	0.016	<d.l.	0.801	49.26	11.39	1.368	1.225	0.646	0.094	7.828	0.012	39.30
TR7	3.95	0.67	455	13.1	0.294	0.067	0.624	246	25	2.2	30	5.1	0.704	7.096	0.016	<d.l.	0.799	49.18	10.80	1.337	1.211	0.577	0.094	7.877	0.013	38.70
TR6	3.93	0.65	469	13.2	0.181	0.062	0.592	228	24	2.3	27	5.1	0.679	7.192	0.014	<d.l.	0.775	48.33	11.09	1.339	1.204	0.829	0.090	7.679	0.014	38.06
TR5	3.87	0.67	453	13.3	0.262	0.082	0.674	193	24	3	35	5	1.051	7.779	0.017	<d.l.	0.803	55.42	11.10	1.578	1.357	0.847	0.104	8.381	0.012	46.95
TR4	3.68	1.09	435	13.3	0.297	0.182	1.418	461	25	4.3	81	5.1	2.860	9.302	0.021	0.086	0.946	64.17	12.26	1.918	1.614	0.734	0.137	10.14	0.013	57.68
TRX	4.76	14.0	287	12.6	<d.l.	4.683	19.69	1623	106	90	2182	4.1	6.223	6.787	0.062	1.340	0.979	67.84	13.71	2.199	2.211	3.309	1.631	10.15	0.015	42.91
TR3	5.13	17.7	222	13.0	1.176	6.063	23.52	1796	123	119	2655	3.3	3.638	2.593	0.068	1.819	0.850	57.84	11.92	1.756	1.841	2.656	2.196	8.384	0.017	26.34
TR2	5.59	23.8	202	12.8	<d.l.	8.968	33.89	1775	161	174	3902	2.6	1.797	0.934	0.080	2.706	0.672	42.02	10.30	0.878	1.235	2.273	3.172	7.107	0.015	10.44
TR1	6.32	32.1	167	12.5	<d.l.	14.47	54.63	3023	243	288	6609	1.3	0.030	<d.l.	0.117	4.198	0.363	18.57	5.651	0.178	0.469	1.622	5.120	2.934	0.013	1.225
GBL	4.52	0.37	328	16.0	0.434	0.012	0.931	257	12	0.9	14	5.20	0.001	3.394	0.007	<d.l.	0.627	30.43	20.79	0.677	1.555	0.507	0.034	4.045	0.014	2.338
O14	4.66	0.49	330	14.6	0.381	0.042	<d.l.	269	16	<d.l.	20	6.4	1.005	6.681	0.015	<d.l.	1.159	44.51	19.94	0.942	1.356	0.443	0.048	6.850	0.013	2.187
O12	4.67	0.59	323	14.8	0.453	0.070	0.519	270	17	2.2	31	6.5	1.107	6.425	0.014	<d.l.	1.186	45.94	20.94	0.958	1.395	0.563	0.060	6.905	0.015	2.382
O9	4.75	0.65	322	14.3	0.660	0.116	0.661	276	17	1.8	42	6.3	1.060	5.791	0.017	<d.l.	1.188	44.69	20.23	0.916	1.379	0.504	0.068	6.931	0.014	2.338
OX	5.21	9.40	n.a.d.	15.1	<d.l.	3.058	10.64	496	67	60	1369	4.8	0.886	1.971	0.036	0.982	1.007	34.94	17.61	0.610	1.430	0.741	1.079	5.659	0.018	1.696
O8	5.77	14.0	200	15.3	<d.l.	4.566	15.19	770	98	101	2182	4	0.578	0.684	0.050	1.521	0.882	30.49	15.63	0.422	1.227	0.629	1.713	4.744	0.017	0.960
OZ	6.35	23.9	217	14.8	<d.l.	8.840	30.48	1194	159	186	3876	2.7	0.061	<d.l.	0.079	2.466	0.649	23.60	11.58	0.210	0.818	0.699	3.120	3.859	0.016	0.303
O2	6.95	34.0	213	15.1	<d.l.	12.51	44.22	1465	208	247	5562	1.7	0.009	0.008	0.107	3.706	0.475	19.14	8.314	0.121	0.561	1.336	4.456	3.187	0.014	0.347
O1	7.12	39.1	198	15.9	<d.l.	15.30	50.79	1848	237	286	6105	1.3	0.012	0.059	0.116	3.814	0.364	14.64	6.144	0.084	0.407	1.573	4.832	2.456	0.014	0.362
C8	7.15	42.8	161	13.7	<d.l.	15.40	58.69	3804	263	294	6804	1.2	0.014	<d.l.	0.120	3.891	0.311	14.55	5.486	0.088	0.282	1.897	5.177	2.198	0.011	0.438
C7	7.03	42.8	292	14.9	<d.l.	16.15	60.52	2772	264	303	7423	0.95	0.017	0.086	0.134	4.921	0.280	12.69	5.195	0.068	0.317	2.056	5.785	2.218	0.012	0.610
C5	7.66	42.7	241	14.4	<d.l.	18.22	64.76	2549	298	344	7746	0.58	0.009	0.154	0.140	4.974	0.187	8.567	3.258	0.041	0.196	1.991	6.345	1.368	0.010	0.321
C4	7.68	43.7	226	13.8	<d.l.	17.32	61.56	2266	278	339	7668	0.74	0.003	<d.l.	0.134	4.944	0.231	10.07	3.730	0.047	0.251	1.854	6.017	1.801	0.010	0.293
C3	7.83	45.7	258	14.0	<d.l.	18.84	65.40	2395	286	357	8027	0.49	0.003	<d.l.	0.133	5.153	0.162	7.568	2.900	0.037	0.181	1.877	6.514	1.320	0.010	0.264
C2	8.05	53.0	219	14.0	<d.l.	12.23	71.82	2709	324	407	8857	0.06	0.006	0.041	0.163	5.866	0.069	3.055	1.510	0.018	0.090	1.944	7.368	0.510	0.008	0.299
C1	8.11	55.6	219	14.4	<d.l.	22.35	74.39	2795	343	423	9297	<d.l.	0.005	<d.l.	0.150	6.033	0.023	1.066	0.897	0.008	0.034	1.729	7.637	0.209	0.007	0.180

n.a.d. non available data.
d.l. detection limit.

PHREEQC code was also used to check speciation of the free ions of interest at the studied pH range.

3. Results

3.1. Seasonal and spatial evolution of contaminants

3.1.1. Low-flow period

Concentrations of major elements and metal(loid)s were monitored at two dry periods, before (May 2018; Tables 1 and S1) and after summer (November 2018; Tables S3 and S4), with the contaminants behaving similarly during both periods. For that reason, tables and figures corresponding to the sampling campaign of November 2018 are given in the Supplementary material (Figs. S1 and S2; Tables S3 and S4). However, the contaminants of interest are more concentrated during November due to the washing of evaporitic salts and sulfide oxidation products that take place with the first rainfalls after summer. The pH evolution and the distribution of the contaminants of interest during the mixing of the acidic river waters with seawater along the estuary of Huelva at the low-flow period (May 2018), is described in Fig. 3. Elemental concentrations (expressed as % ratio) corresponding to the dissolved and the particulate fractions, are presented to show the mobility of the contaminants. Before summer and at low-flow conditions (May 2018), the pH values were highly acidic at both the Tinto (up to 2.9; Figs. 2 and 3; Table 1) and the Odiel river waters (up to 4.2; Figs. 2 and 3; Table 1), until reaching the estuaries, where the mixing with seawater occurs (Fig. 2). After entering the mixing zone, the pH started to increase from acidic to alkaline values of up to 7.6 at both systems (Fig. 3; Table 1) due to dilution and acid neutralization with seawater. The increasing influence of seawater is reflected in the pH conditions and the elements concentrations (Figs. 3 and S1; Table 1). In the common estuarine channel (points C8 to C1; Fig. 2), waters reached pH values of almost 8 (Fig. 3), having chiefly a seawater influence. Total Fe concentrations were much higher at the Tinto estuary compared to Odiel (Fig. S1) for all the sampling periods, as expected due to its higher AMD influence. The concentration of Fe in solution decreased to the mouth of the estuary, not only by dilution, but also probably because of Fe precipitation. Thus, Fe passes from being over 80 % in the dissolved fraction (up to points TR4 and O12) to almost 100 % in the particulate fraction, already before entering the confluence of the two rivers (Figs. 2 and 3). In particular, Fe was initially, mostly present in its dissolved form at both rivers (Fig. 3). However, following the pH increase, dissolved Fe decreased down to 1–1.5 % before the confluence of the two estuaries (see Fig. 1). Before entering the ocean, a slightly increase of dissolved Fe (up to 12 %) was also observed (Fig. 3).

Arsenic, which was mostly present in solution at the Tinto and Odiel rivers, showed an "*on-off*" behavior along the estuaries during seawater mixing (Fig. 3), meaning that while As was initially removed from solution, it was remobilized at certain conditions. This behavior is surmised by As removal from solution together with Fe, and a subsequent increase of the dissolved fraction at circumneutral pH values, until reaching again 100 % (Fig. 3). Arsenic concentration in solution passed to the particulate fraction already at pH around 3 at the Tinto (Fig. 3A; Table 1) and at pH around 4 at the Odiel estuary (Fig. 3B; Table 1). Total As concentrations were lower before summer (March 2018; Fig. S1; Table S1) compared to the post-summer sampling event (November 2018; Fig. S1; Table S4). As such, the dissolved fraction of As reached much lower values after summer, i.e. down to 24 % of the total As for Tinto (Fig. S2A), and 40 % for Odiel (Fig. S2B), compared to the pre-summer period when the dissolved As did not fall below 50 % with respect to the total concentration (Fig. 3). However, at the confluence of the two rivers (C1–5) and at pH values >7.5, the previously retained As

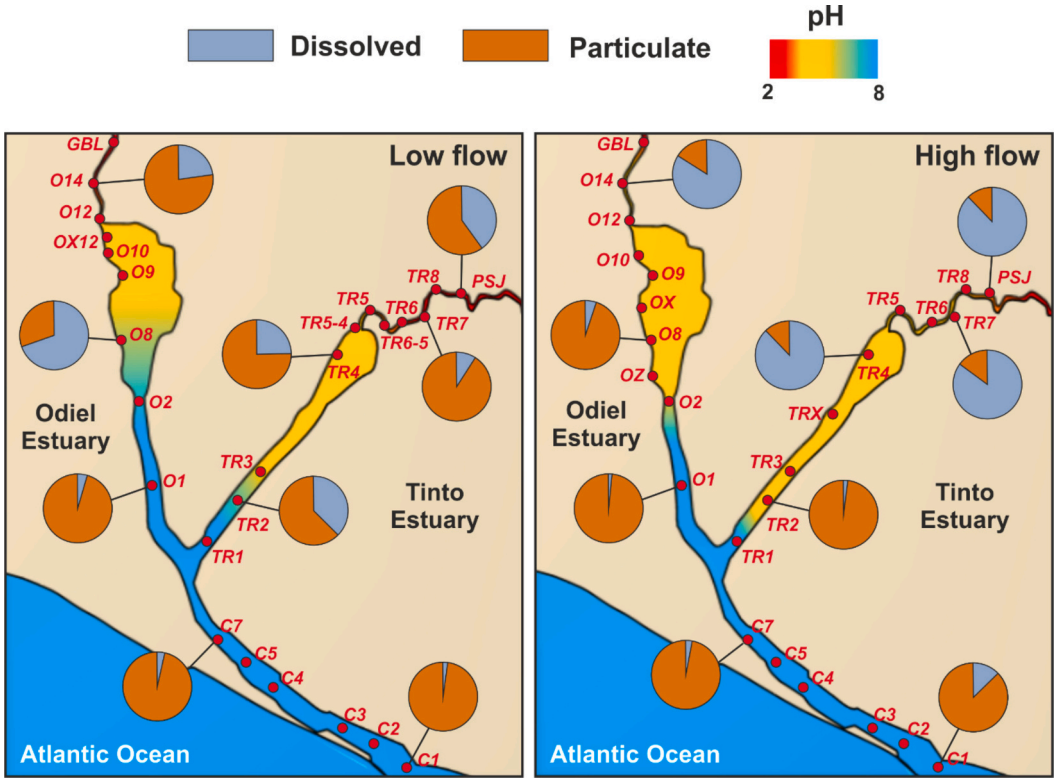

Fig. 2. Sketch maps of the sampling locations, including the proportion of the dissolved and particulate Fe concentrations for selected samples (pie diagrams). The color degradation of the river and estuarine waters illustrates the pH evolution from highly acidic to alkaline values during estuarine mixing and AMD neutralization (from red to blue), demonstrating the entire mixing zones of the Tinto and Odiel Estuaries Left: Data corresponding to the low-flow sampling campaign (May 2018); right: data corresponding to the high-flow sampling campaign (March 2018).

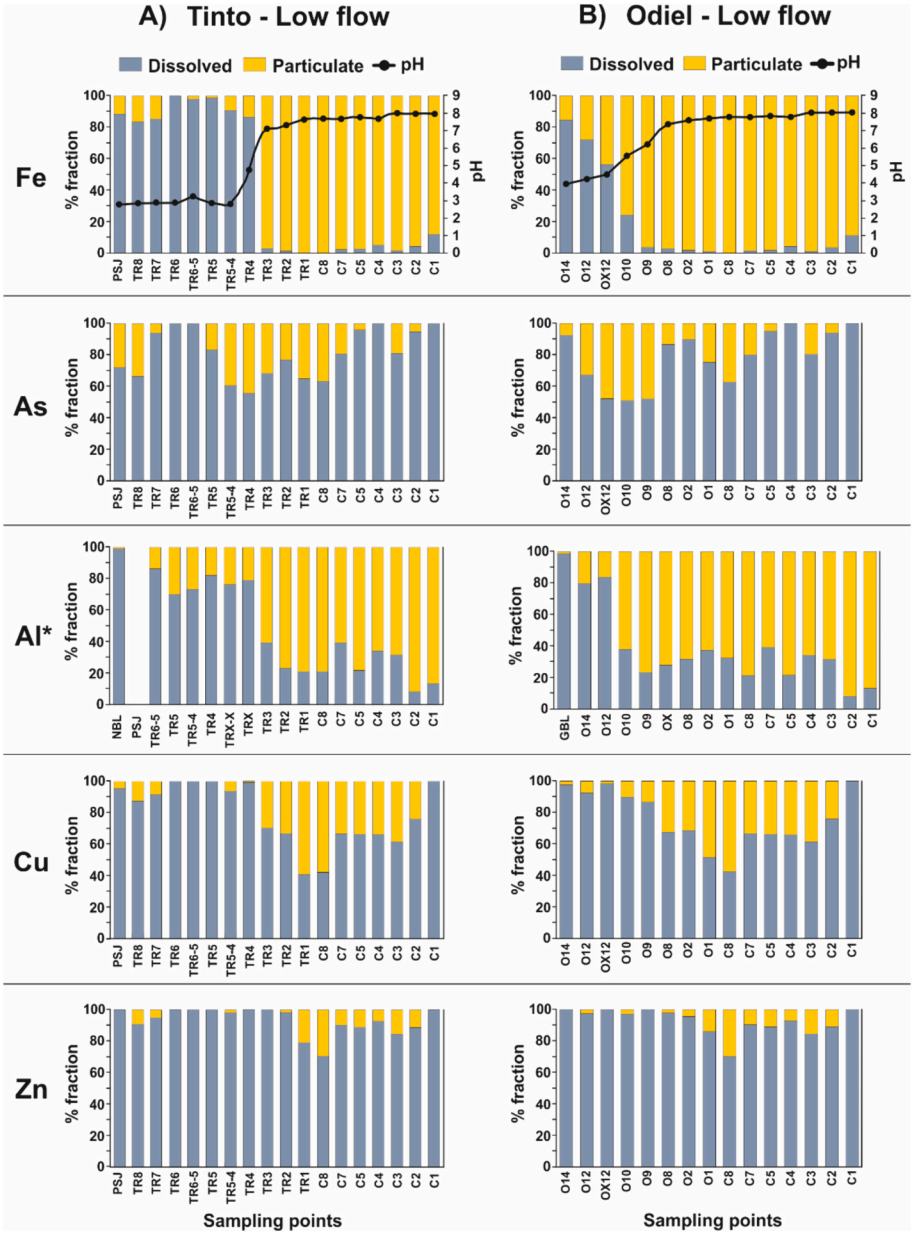

Fig. 3. Evolution of dissolved (grey bars) and particulate (yellow bars) ratios (expressed in %) of Fe, As, Al, Cu, and Zn along the (A) Tinto and (B) Odiel estuaries, during the sampling event of May 2018, corresponding to a low-flow/dry period. The pH evolution is also represented with the distribution of Fe (black pointed line). The asterisk (*) in the case of Al indicates the use of data corresponding to the sampling of November 2018 as an exception, due to limited Al data from the sampling of May 2018.

in the particulate matter, appeared to return to the dissolved fraction due to desorption processes, to eventually occupying 100 % of the total As, and ending as such to the ocean (Fig. 3).

Metals such as Al, Pb, and to a lesser extent, Cu seem to follow also a non-conservative behavior at the estuarine waters. Thus, the decrease in their total concentrations may be not only because of the dilution by seawater, but also by mineral precipitation. This non-conservative behavior can be deduced since the % dissolved fraction with respect to the total decrease during water mixing result from the precipitation of those elements passing to the particulate matter fraction (increased particulate fraction) (Fig. 3). For instance, the removal of Al from solution appeared to be quite efficient, with the dissolved fraction reaching <20 % of the total concentration (Fig. 3), while the dissolved concentration of Cu did not fall below 40 % (Fig. 3). In fact, Cu returned entirely to solution during May (Fig. 3) and at 80 % in November (Fig. S2), right before entering the oceanic environment, similarly to As, and evidencing potential desorption processes.

Decreasing in their total concentrations along the estuary, elements such as Zn, Cd, Mn, Co and Ni seem to have a quasi-conservative behavior, which may be exclusively associated with the dilution effect by seawater. Null to minimal precipitation occurred as most of the total concentration of these elements was dominated by the dissolved fraction (e.g. Zn in Fig. 3). This interpretation is based on particulate-dissolved partitioning with the sampled water column, however particulate material is subject to settling and resuspension, decoupling its transport dynamics from dissolved species in estuaries. For this reason, this issue will be discussed in depth in the Discussion section.

3.1.2. High-flow period

The evolution of pH and the mobility of contaminants is illustrated in Fig. 4, similarly to the low-flow periods. The pH values on Tinto and Odiel rivers, after a rainy period (March 2018), were higher compared to the drier sampling periods, with values up to ~4 and ~ 4.5, respectively. These values gradually increased while mixing with seawater up to pH 8 before reaching the ocean (Fig. 4; Table 2). As expected, total and dissolved concentrations of most contaminants at both estuaries were lower compared to the low-flow periods due to dilution with rainwater, and consequently, higher estuarine water flow (Figs. 4 and S1). Total Fe concentrations were higher at the Tinto Estuary compared to Odiel (Fig. S1), similarly to the low-flow sampling periods. The increasing pH trend was correlated with a significant reduction of the of dissolved Fe (Fig. 4) down to around 1 % of the total Fe during estuarine mixing, associated with Fe precipitation (Fig. 4). However, at this wet period, a zone of Fe redissolution was observed at both estuaries at a pH range between 3.6 and 5.8, where part of the precipitated Fe returned shortly to the dissolved fraction. Thereafter, an almost complete transfer of Fe to the particulate matter occurs, in the confluence channel before the open littoral waters (Fig. 4).

The behavior of As was more particular during the period following rains and flooding events. On the contrary to the dry periods, As entered the estuarine mixing zones already sorbed onto Fe minerals, with almost 100 % present in the particulate matter, when solutions were at a pH range between 4 and 5 (Fig. 4). When estuarine waters approached closer to circumneutral pH values, As started to desorb from the precipitated phases, similarly to the low-flow periods, until it was completely dissolved, ending up as such in the ocean (Fig. 4). Desorption of As at the Odiel estuary started at lower pH (~5.2, point OX; Fig. 4B; Table 2) compared to the Tinto, where it was more evident at pH around 7, right before mixing with the Odiel estuarine waters (TR1–3; Figs. 2 and 4A) in the common channel.

Equally observed during the low-flow sampling campaigns, the respective dissolved fraction of Al, Cu, and Pb at both rivers, decreased

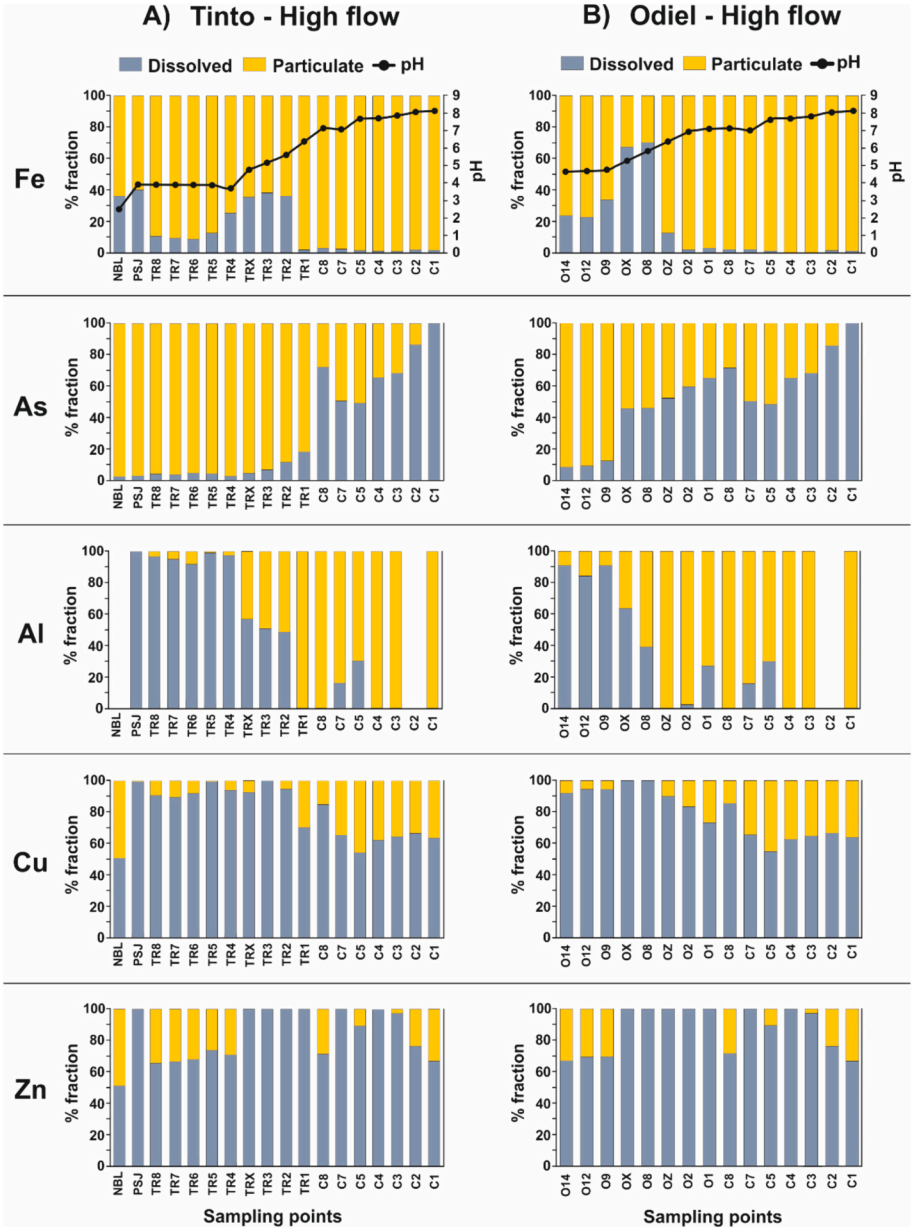

Fig. 4. Evolution of dissolved (grey bars) and particulate (yellow bars) ratios (expressed in %) of Fe, As, Al, Cu, and Zn along the (A) Tinto and (B) Odiel estuaries, during the sampling event of March 2018, corresponding to a high-flow/wet period. The pH evolution is also represented alongside the distribution of Fe (black pointed line).

notably during estuarine mixing not only by dilution, but also by precipitation processes. The dissolved fraction of Al was reduced below 50 % after estuarine mixing at both systems, and virtually 100 % of the total Al that ended up to the ocean was present in the particulate matter (Fig. 4). Dissolved Cu decreased down to 70 % before the confluence of both estuaries, and down to 64 % when entering the ocean (Fig. 4). However, Cu did not appear to participate in desorption processes at the confluence of both estuarine systems as observed in the dry periods, and thus, a great Cu fraction remained immobilized before reaching the ocean.

Conversely, the greatest part of the total concentrations of Zn, Cd, Mn, Co and Ni was present in their dissolved fraction through the entire estuarine system (e.g. Zn in Fig. 4). This suggests that these metals may behave conservatively during mixing with seawater, and their participation in adsorption processes may be insignificant, as also described for the low-flow periods. However, an increase in the Zn concentration in the particulate phase, with respect to the total concentrations was observed at both estuaries, and predominantly at the beginning of the estuarine mixing zones (points TR8-TR4, and O14-O9; Fig. 4).

4. Discussion

4.1. Sorption of contaminants

Metal partitioning between solid and aqueous phase described in Results section suggest the existence of elements affected by precipitation/sorption processes in the estuary. However particulate material is subject to settling and resuspension, decoupling its transport dynamics from dissolved species in estuaries, thus a deeper insight must be provided in these processes. The concentration of Fe in solution decreased to the mouth of the estuary, not only by dilution, but also because of Fe (III) mineral precipitation. According to PHREEQC code simulations, fluvial AMD and estuarine solutions at both low- and high-flow periods were supersaturated with respect to Fe(III) mineral phases such as goethite (FeOOH), hematite (Fe_2O_3), jarosite ($KFe_3(SO_4)_2(OH)_6$), jarosite-Na ($NaFe_3(SO_4)_2(OH)_6$), and schwertmannite ($Fe_8O_8(SO_4)_{1.5}(OH)_5$) (Tables S5 and S6). Ideal reactions and equilibrium constants of those phases are given in Table S7. Among them, schwertmannite, a common mineral formed in AMD environments under high sulfate concentration and acidic conditions (Bigham et al., 1994; Bigham and Nordstrom, 2000; Burton et al., 2009), may be the predominant mineral in these waters. Thus, during estuarine AMD neutralization (pH 2.5–6) the dissolved Fe precipitated mainly as schwertmannite, as suggested by the solid phase analysis (Fig. 5A). Apart from the most important mineral phase for Fe solubility, schwertmannite appears to be the major sorbent of the present toxic elements, favoring their natural attenuation while forming processes (Smith, 1999; Espana et al., 2005). The short Fe increase observed at the high-flow period before Fe returned to the particulate phase, could be related to the redissolution of Fe-rich particles carried by particulate matter with the sharp increase in salinity (Achterberg et al., 2003; Carro et al., 2011).

With respect to As, the decrease in dissolved concentration is in concert with the pH increase, as well as the decrease of the dissolved Fe, which suggests As sorption processes on iron phases (Fig. 3). Iron (oxyhydr)oxides in general, are known for their high sorption affinity towards As species over a wide pH range (Dixit and Hering, 2003), while schwertmannite is considered one of the most efficient solid phases in removing As from acidic waters (Carrero et al., 2015). Here, precipitation of schwertmannite led to the adsorption of the dissolved As at pH values in the range of 3 to 6 (Figs. 3 and 4), in accordance with various studies in the Huelva estuary and in similar acidic environments worldwide (e.g. Carlson et al., 2002; Fukushi et al., 2004; Asta et al., 2010; Parviainen et al., 2015). However, when estuarine waters reached pH values higher than schwertmannite's zero-point charge (pHpzc = 7.2 (Jönsson et al., 2005)), As was desorbed from those phases, returning entirely to the dissolved fraction (Figs. 3 and 4), in agreement with previous studies (Olías et al., 2006; Burton et al., 2009; Hierro et al., 2014). Apart from the pH conditions, As sorption to Fe minerals is controlled by its speciation. In this sense, in the studied system, As is present almost entirely in its pentavalent form, which has been confirmed by its speciation suggested by PHREEQC, as also, reported to previous studies (e.g. Asta et al., 2010). Therefore, the efficiency of As sorption at lower pH than the pHpzc of schwertmannite can be explained by considering the predominant anionic species of aqueous As (V) in the studied environment ($H_2As^VO_4^-$ and $HAs^VO_4^{2-}$) and their strong affinity to the abundant, positively charged sorption sites of schwertmannite (Burton et al., 2009; Pérez-López et al., 2023). Nevertheless, at higher pH values (>pzc of schwertmannite) the respective sorption sites have negative charge, and thus, no affinity for the aforementioned As species due to electrostatic repulsion, resulting to their mobilization. This process would explain the "*on-off*" As behavior, that is, the schwertmannite that flocculates in the estuary adsorbed As (OFF) below a pH value about 5.0. However, the As would be desorbed (ON), passing again to solution, when these precipitates reached the estuarine zones with pH values above 6.5. In addition, the elevated dissolved carbonate as seawater influence increases, could be displacing the sorbed As from the precipitated minerals (Appelo et al., 2002; Hierro et al., 2014).

The higher As concentration in the estuary during November compared to May may be caused by the washing of evaporitic salts and metal-rich pore waters in mine sites. There is a delay of As peak

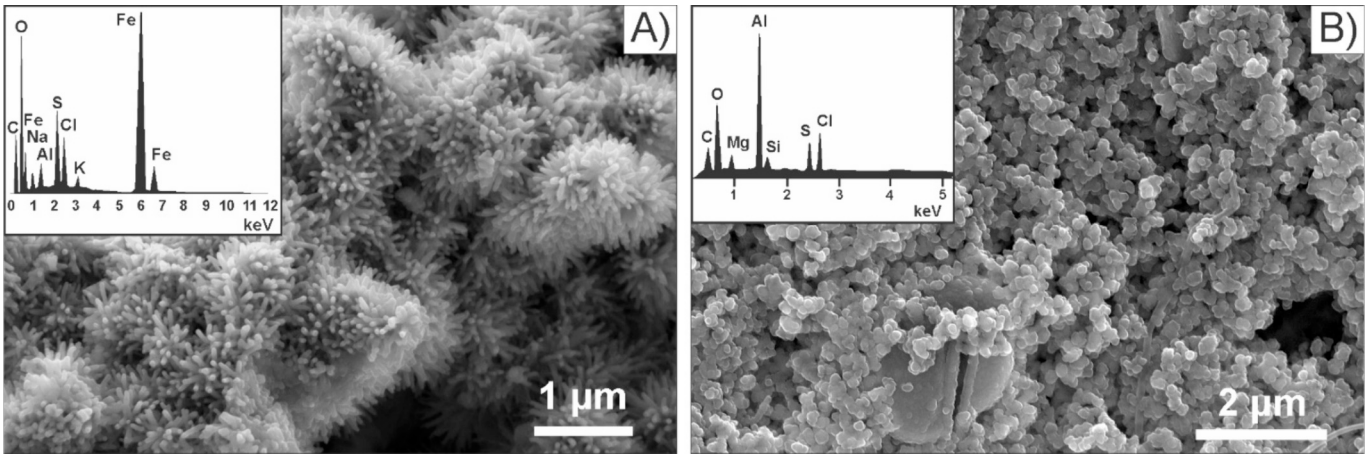

Fig. 5. Scanning electron microscopy images and energy dispersive spectroscopy spectra of precipitates collected from representative samples, corresponding to A) schwertmannite (sample TR4, low-flow period), and B) basaluminite (sample O9, low-flow period).

regarding the rest of AMD-related elements (1 or 2 month afterwards of rainfall onset). Under the post-summer regime, the river waters residence time is much higher and As sorption processes more intense ((Cánovas et al., 2010)). The fluctuations of dissolved As at the confluence of the Tinto and Odiel estuaries (from C8 to C1; Fig. 3), despite its general increasing trend, are attributed to the mixing of two distinct estuarine waters, with different chemical characteristics and load of contaminants, leading to shifting As adsorption/desorption processes. Finally, the sorption of As at the high-flow period at an earlier stage is explained by the rainy events resulting in higher rivers flow, and consequently, higher pH values before estuarine mixing.

In regard to Al and according to geochemical calculations, solutions were supersaturated with respect to phases such as alunite ($KAl_3(SO_4)_2(OH)_6$), gibbsite ($Al(OH)_3$), and basaluminite ($Al_4(OH)_{10}SO_4$) (Tables S5 and S6), with the latter being the main mineral that controls Al solubility in the presented acidic system (Espana et al., 2005). This is in concert with SEM-EDS analysis that suggested basaluminite as the prevalent Al mineral at the suspended material, based on the morphology of the particulate matter and the respective chemical analysis (Fig. 5B). Therefore, the Al decreasing in solution during estuarine mixing at pH 4.7–6 (Figs. 3 and 4), is attributed to its precipitation as basaluminite, which occurred after Fe precipitation, in agreement with other studies (Lozano et al., 2020). As such, the first buffer (pH 2.5–6) in the mixing waters coincides with Fe(III) precipitation, followed by a second buffer (pH 4.7–6) corresponding to Al precipitation, also observed in laboratory simulations of the same system (Pérez-López et al., 2023).

Although characterization of the particulate material showed that Al precipitates are less abundant than those of Fe (Fig. 5B), basaluminite plays an important role in the behavior of other occurring metal(loid)s, such as As and Cu (Carrero et al., 2017), which show a high affinity for this Al mineral, especially in AMD environments (Bigham and Nordstrom, 2000; Carrero et al., 2015; Pérez-López et al., 2023). As such, and considering the simultaneous decrease of dissolved Cu with Al (Figs. 3 and 4), the increase of the Cu concentration in the particulate phase during estuarine mixing could be attributed to adsorption and/or coprecipitation process with basaluminite. These processes are favored by Cu speciation that is mostly present as Cu(II) in the studied waters, as confirmed by PHREEQC modelling for both low- and high-flow samples. However, the following rapid desorption of Cu at the low-flow periods could be explained by the sharp salinity change, known as 'salinity shock' caused by the introduction of the particulate matter originating from a low salinity environment, into seawater, with a consequent competition for metal binding ligand sites by major seawater cations (Achterberg et al., 2003; Kerl et al., 2023). Although basaluminite is considered a strong sorbent also for As, its sorption capacity is masked by the previously occurred schwertmannite precipitation (Carrero et al., 2015).

Seawater mixing experiments of acidic leachates from Tinto and Odiel rivers were previously performed in the laboratory, following a controlled pH increase and simulating the real field conditions at the estuarine mixing zone. The respective results confirm the non-conservative or "*on-off*" behavior of contaminants such as Fe, As, Al, and Cu, showing that is controlled by sorption process mainly onto schwertmannite and basaluminite (Pérez-López et al., 2023).

4.2. Conservative contaminants

On the other hand, the conservative trend of certain metals is explained by the formation of ion complexes in the studied pH range that do not favor their partitioning in the precipitated solid phases (Papaslioti et al., 2018b), since their adsorption to Fe minerals is strongly pH dependent. The role of pH is combined with the effect of surface charge of the precipitated particles and the protonation of their adsorption sites that is repellent to the positive charges of the free Zn, Cd, Mn, Ni, and Co ions (Achterberg et al., 2003; Braungardt et al., 2003; Yaciuk et al., 2022). The positive charge of the predominant species of those metals agrees with the speciation predicted by PHREEQC modelling conducted for the presented data (i.e., Zn^{2+}, Cd^{2+}, Mn^{2+}, Ni^{2+}, and Co^{2+}). Even when alkaline pH was reached, their sorption should be inhibited by the antagonistic effect of major cations present in the seawater, such as Ca^{2+} and Mg^{2+}. Complexation of metals with dissolved seawater anions and their competition with the aforementioned major elements, shift the sorption efficiency to higher pH values due to the increase of seawater proportion (Millward and Moore, 1982; Achterberg et al., 2003).

This conservative behavior has been confirmed by laboratory simulations of seawater mixing with AMD solutions from the studied area, showing that their dissolved concentrations are only affected by dilution and not by precipitation processes (Pérez-López et al., 2023). Fig. S3 exhibits the evolution of Fe and Zn against chlorinity along the estuary upon high- and low-flow conditions. As can be seen, those elements follow a different trend, highlighting the non-conservative behavior of Fe compared to other cations such as Zn, Cd, Ni or Co. The observed conservative behavior of Cd in the present research is in accord with a recent study on Cd and Zn isotopes (Packman et al., 2023). However, our results are not in line with this study regarding Zn, as they document a removal of 49–97 % of the dissolved riverine fraction in the estuary. This could be explained by the higher pH values (~8.8) registered during their respective sampling periods that may have favored Zn partitioning to the particulate matter. In this context, the lack of reactivity of the studied elements contributes to the high dissolved metal concentrations observed in the Gulf of Cádiz, and subsequently to the Atlantic Ocean, as also supported in similar seawater mixing by previous studies (Papaslioti et al., 2018b; Pérez-López et al., 2023). Although it is not clear in the present data, a possible influence from the adjacent large phosphogypsum stacks to the behavior of the studied contaminants, cannot be discarded, as shown by previous isotope studies, i.e. for Cd (Packman et al., 2023).

The increase of Zn in the particulate phase during the high-flow period at the beginning of the estuarine mixing zones (Fig. 4) is associated to coprecipitation/adsorption processes to Fe phases due to the high load of particulate material carried by the rivers and entering the estuaries as a consequence of river flooding, as was the case described by Packman et al. (2023). Thus, the increase of Zn in the particulate phase at those sampling areas coincides with that of Fe (Fig. 4).

5. Conclusions

The Tinto and Odiel estuaries are among the most heavily AMD affected areas worldwide, draining highly acidic waters, rich in various potentially toxic elements, with Tinto demonstrating more extreme conditions. When the acidic waters enter the estuarine mixing zone, they are subjected to a gradual pH increase and to a subsequent decrease in the dissolved concentrations of various contaminants by dilution with seawater and/or by precipitation processes. The studied estuarine environment is also, subjected to seasonal variations (low-flow/high-flow) that control the geochemical processes along the mixing zones. The evolution of the physicochemical parameters between the two estuaries was similar, with slightly higher pH values at least through the Odiel estuary during the high-flow season. After the confluence of the two estuaries, the pH reached a value around 8 before entering the oceanic environment.

Following the evolution of the pH and the increase of the seawater influence towards the ocean, the behavior of the major metal(loid)s present in the estuarine waters, varied (entirely or partly) among non-conservative, "*on-off*" or conservative. Iron and Al, regarded as the major mining-related metals in the estuaries, were non-conservative with a removal up to 90 % and 100 % from the solution during the low-flow and the high-flow periods, respectively, owing to their precipitation. The solubility of Fe and Al was driven mainly by the formation of schwertmannite and basaluminite, respectively, controlling the sorption processes of the studied non-conservative trace elements in

solution, and highlighting the importance of their precipitation in metal fluxes to ocean.

During the low-flow periods, As was removed from solution up to 70 % following the pH increase due to adsorption to schwertmannite, but it was entirely desorbed from the particulate phase at pH > pzc of the Fe mineral. The same occurred during the high-flow season, although the greatest part of As entered the estuarine mixing zone already sorbed to schwertmannite. Copper was only partially removed from solution at around 50 % during both periods, sorbed to basaluminite, although it was fully desorbed before entering the ocean, at the pre-summer, low-flow period.

On the contrary, Zn, Cd, Mn, Ni, and Co showed a conservative behavior almost through the entire estuarine mixing zones, with minimal partitioning to any sorption processes. Consequently, they entered the oceanic environment mostly mobilized along with As and part of Cu, highlighting their contribution of the studied estuarine system to the total contamination of the Atlantic Ocean.

CRediT authorship contribution statement

Evgenia-Maria Papaslioti: Writing – original draft, Visualization, Validation, Methodology, Investigation, Formal analysis. **Manolis Giampouras:** Writing – review & editing, Visualization, Validation, Methodology, Investigation, Formal analysis. **Laura Sánchez-López:** Writing – review & editing, Investigation. **María Dolores Basallote:** Writing – review & editing, Validation, Methodology, Conceptualization. **Rémi Freydier:** Writing – review & editing, Methodology. **Carlos Ruiz Cánovas:** Writing – review & editing, Validation, Methodology, Conceptualization. **Rafael Pérez-López:** Writing – review & editing, Validation, Supervision, Methodology, Funding acquisition, Conceptualization.

Declaration of competing interest

The authors declare that they have no known competing financial interests or personal relationships that could have appeared to influence the work reported in this paper.

Data availability

Data will be made available on request.

Acknowledgements

This work was supported by the research project TRAMPA (PID2020-119196RBC21) funded by MCIN/AEI/10.13039/501100011033. Dr. M. Giampouras acknowledges the 'Juan de la Cierva e Formacion' (FJC2021-048014-I) Fellowship funded by MCIN/AEI/10.13039/501100011033. L. Sánchez-López acknowledges the "Formación de Personal Investigador" grant (PRE2021-097651) funded by MCIN/AEI/10.13039/501100011033. M. D. Basallote thanks the Regional Government of Andalusia for the EMERGIA grant (EMC21_00363) and MCIN for the RYC2022-035326-I grant funded by MCIN/AEI/10.13039/501100011033 and FSE+. C.R Cánovas thanks the Spanish Ministry of Science and Innovation for the Postdoctoral Fellowship granted under application reference RYC2019-027949-I funded by MCIN/AEI/10.13039/501100011033. Universidad de Huelva/CBUA is acknowledged for funding the open access charge.

Appendix A. Supplementary data

Supplementary data to this article can be found online at https://doi.org/10.1016/j.scitotenv.2024.174683.

References

Achterberg, E.P., Herzl, V.M., Braungardt, C.B., Millward, G.E., 2003. Metal behaviour in an estuary polluted by acid mine drainage: the role of particulate matter. Environ. Pollut. 121 (2), 283–292.

Appelo, C.A.J., Van der Weiden, M.J.J., Tournassat, C., Charlet, L., 2002. Surface complex- ation of ferrous iron and carbonate on ferrihydrite and the mobilization of arsenic. Environ. Sci. Technol. 36 (14), 3096–3103.

Asta, M.P., Ayora, C., Román-Ross, G., Cama, J., Acero, P., Gault, A.G., Bardelli, F., 2010. Natural attenuation of arsenic in the Tinto Santa Rosa acid stream (Iberian Pyritic Belt, SW Spain): the role of iron precipitates. Chem. Geol. 271 (1–2), 1–12.

Bewers, J.M., Yeats, P.A., 1989. Transport of river-derived trace metals through the coastal zone. Neth. J. Sea Res. 23 (4), 359–368.

Bigham, J.M., Nordstrom, D.K., 2000. Iron and aluminum hydroxysulfates from acid sulfate waters. In: Alpers, C.N., Jambor, D.K., Nordstrom, D.K. (Eds.), Sulfate Minerals, Reviews in Mineralogy and GeoChemistry. Mineralogical Society of America, Washington, D.C (, 608 p.).

Bigham, J.M., Carlson, L., Murad, E., 1994. Schwertmannite, a new iron oxyhydroxysulphate from Pyhasalmi, Finland, and other localities. Min. Mag. 58 (4), 641–648. https://doi.org/10.1180/minmag.1994.058.393.14.

Braungardt, C.B., Achterberg, E.P., Elbaz-Poulichet, F., Morley, N.H., 2003. Metal geochemistry in a mine-polluted estuarine system in Spain. Appl. Geochem. 18 (11), 1757–1771.

Burton, E.D., Bush, R.T., Johnston, S.G., Watling, K.M., Hocking, R.K., Sullivan, L.A., Parker, G.K., 2009. Sorption of arsenic (V) and arsenic (III) to schwertmannite. Environ. Sci. Technol. 43 (24), 9202–9207.

Cánovas, C.R., Olías, M., Nieto, J.M., Sarmiento, A.M., Cerón, J.C., 2007. Hydrogeochemical characteristics of the Tinto and Odiel Rivers (SW Spain). Factors controlling metal contents. Sci. Total Environ. 373 (1), 363–382.

Cánovas, C.R., Olías, M., Nieto, J.M., Galván, L., 2010. Wash-out processes of evaporitic sulfate salts in the Tinto river: hydrogeochemical evolution and environmental impact. Appl. Geochem. 25 (2), 288–301.

Carlson, L., Bigham, J.M., Schwertmann, U., Kyek, A., Wagner, F., 2002. Scavenging of As from acid mine drainage by schwertmannite and ferrihydrite: a comparison with synthetic analogues. Environ. Sci. Technol. 36 (8), 1712–1719.

Carrero, S., Pérez-López, R., Fernandez-Martinez, A., Cruz-Hernández, P., Ayora, C., Poulain, A., 2015. The potential role of aluminium hydroxysulphates in the removal of contaminants in acid mine drainage. Chem. Geol. 417, 414–423.

Carrero, S., Fernandez-Martinez, A., Pérez-López, R., Poulain, A., Salas-Colera, E., Nieto, J.M., 2017. Arsenate and selenate scavenging by basaluminite: insights into the reactivity of aluminum phases in acid mine drainage. Environ. Sci. Technol. 51 (1), 28–37.

Carro, B., Borrego, J., López-González, N., Grande, J.A., Gómez, T., De la Torre, M.L., Valente, T., 2011. Impact of acid mine drainage on the hydrogeochemical characteristics of the Tinto-Odiel Estuary (SW Spain). J. Iber. Geol. 37 (1), 87–96.

Chalkley, R., Child, F., Al-Thaqafi, K., Dean, A.P., White, K.N., Pittman, J.K., 2019. Macroalgae as spatial and temporal bioindicators of coastal metal pollution following remediation and diversion of acid mine drainage. Ecotoxicol. Environ. Saf. 182, 109458.

de Souza Machado, A.A., Spencer, K., Kloas, W., Toffolon, M., Zarfl, C., 2016. Metal fate and effects in estuaries: a review and conceptual model for better understanding of toxicity. Sci. Total Environ. 541, 268–281.

Dixit, S., Hering, J.G., 2003. Comparison of arsenic (V) and arsenic (III) sorption onto iron oxide minerals: implications for arsenic mobility. Environ. Sci. Technol. 37 (18), 4182–4189.

Espana, J.S., Pamo, E.L., Santofimia, E., Aduvire, O., Reyes, J., Barettino, D., 2005. Acid mine drainage in the Iberian Pyrite Belt (Odiel river watershed, Huelva, SW Spain): geochemistry, mineralogy and environmental implications. Appl. Geochem. 20 (7), 1320–1356.

Fukushi, K., Sato, T., Yanase, N., Minato, J., Yamada, H., 2004. Arsenate sorption on schwertmannite. Am. Mineral. 89 (11–12), 1728–1734.

Grande, J.A., Borrego, J., Morales, J.A., De la Torre, M.L., 2003. A description of how metal pollution occurs in the Tinto–Odiel rias (Huelva-Spain) through the application of cluster analysis. Mar. Pollut. Bull. 46 (4), 475–480.

Guerrero, J.L., Pérez-Moreno, S.M., Gutiérrez-Álvarez, I., Gázquez, M.J., Bolívar, J.P., 2021. Behaviour of heavy metals and natural radionuclides in the mixing of phosphogypsum leachates with seawater. Environ. Pollut. 268, 115843.

Hierro, A., Olías, M., Ketterer, M.E., Vaca, F., Borrego, J., Cánovas, C.R., Bolivar, J.P., 2014. Geochemical behavior of metals and metalloids in an estuary affected by acid mine drainage (AMD). Environ. Sci. Pollut. Res. 21, 2611–2627.

Johnson, J., Anderson, G., Parkhurst, D., 2000. Database thermo. com. Com. Lawrence Livermore National Laboratory, Livermore, California.

Jönsson, J., Persson, P., Sjöberg, S., Lövgren, L., 2005. Schwertmannite precipitated from acid mine drainage: phase transformation, sulphate release and surface properties. Appl. Geochem. 20 (1), 179–191.

Kerl, C.F., Basallote, M.D., Käberich, M., Oldani, E., Espejo, N.P.C., Blanco, A.E.C., Cánovas, C.R., Nieto, J.M., Planer-Friedrich, B., 2023. Consequences of sea level rise for high metal (loid) loads in the Ría of Huelva estuary sediments. Sci. Total Environ. 873, 162354.

Liang, Y., Wong, M.H., 2003. Spatial and temporal organic and heavy metal pollution at Mai Po Marshes Nature Reserve. Hong Kong. Chemosphere 52 (9), 1647–1658.

Lozano, A., Ayora, C., Macías, F., León, R., Gimeno, M.J., Auqué, L., 2020. Geochemical behavior of rare earth elements in acid drainages: modeling achievements and limitations. J. Geochem. Explor. 216, 106577.

Martín-Ramos, J.D., 2004. Using XPowder: A Software Package for Powder X-ray Diffraction Analysis, D.L. GR-1001/04 84-609-1497-6, Spain.

Mayes, W.M., Jarvis, A.P., 2016. Mine water outbreak and stability risks: examples and challenges from England and Wales. Proceedings of IMWA 1078–1083.
Millward, G.E., Moore, R.M., 1982. The adsorption of Cu, Mn and Zn by iron oxyhydroxide in model estuarine solutions. Water Res. 16 (6), 981–985.
Nieto, J.M., Sarmiento, A.M., Olías, M., Canovas, C.R., Riba, I., Kalman, J., Delvalls, T.A., 2007. Acid mine drainage pollution in the Tinto and Odiel rivers (Iberian Pyrite Belt, SW Spain) and bioavailability of the transported metals to the Huelva Estuary. Environ. Int. 33 (4), 445–455.
Nieto, J.M., Sarmiento, A.M., Canovas, C.R., Olias, M., Ayora, C., 2013. Acid mine drainage in the Iberian Pyrite Belt: 1. Hydrochemical characteristics and pollutant load of the Tinto and Odiel rivers. Environ. Sci. Pollut. Res. 20, 7509–7519.
Nocete, F., Álex, E., Nieto, J.M., Sáez, R., Bayona, M.R., 2005. An archaeological approach to regional environmental pollution in the south-western Iberian Peninsula related to Third millennium BC mining and metallurgy. J. Archaeol. Sci. 32 (10), 1566–1576.
Nordstrom, D.K., Wilde, F.D., 1998. Reduction-oxidation potential (electrode method), section 6.5, chapter A6. In: National Field Manual for the Collection of Water-quality Data, p. 20. https://doi.org/10.3133/twri09A6.5.
Olías, M., Cánovas, C.R., Nieto, J.M., Sarmiento, A.M., 2006. Evaluation of the dissolved contaminant load transported by the Tinto and Odiel rivers (South West Spain). Appl. Geochem. 21 (10), 1733–1749.
Packman, H., Little, S.H., Nieto, J.M., Basallote, M.D., Pérez-López, R., Coles, B., Rehkämper, M., 2023. Tracing acid mine drainage and estuarine Zn attenuation using Cd and Zn isotopes. Geochim. Cosmochim. Acta 360, 36–56.
Papaslioti, E.M., Pérez-López, R., Parviainen, A., Macías, F., Delgado-Huertas, A., Garrido, C.J., Nieto, J.M., 2018a. Stable isotope insights into the weathering processes of a phosphogypsum disposal area. Water Res. 140, 344–353.
Papaslioti, E.M., Pérez-López, R., Parviainen, A., Sarmiento, A.M., Nieto, J.M., Marchesi, C., Garrido, C.J., 2018b. Effects of seawater mixing on the mobility of trace elements in acid phosphogypsum leachates. Mar. Pollut. Bull. 127, 695–703.
Parkhurst, D.L., Appelo, C.A.J., 2013. Description of input and examples for PHREEQC version 3—a computer program for speciation, batch-reaction, one-dimensional transport, and inverse geochemical calculations. In: US Geological Survey Techniques and Methods, Book 6, chap A43, p. 497. https://pubs.usgs.gov/tm/06/a43/.
Parviainen, A., Cruz-Hernández, P., Pérez-López, R., Nieto, J.M., Delgado-López, J.M., 2015. Raman identification of Fe precipitates and evaluation of As fate during phase transformation in Tinto and Odiel River Basins. Chem. Geol. 398, 22–31.
Pérez-López, R., Nieto, J.M., López-Cascajosa, M.J., Díaz-Blanco, M.J., Sarmiento, A.M., Oliveira, V., Sánchez-Rodas, D., 2011. Evaluation of heavy metals and arsenic speciation discharged by the industrial activity on the Tinto-Odiel estuary. SW Spain. Marine Pollution Bulletin 62 (2), 405–411.
Pérez-López, R., Macías, F., Cánovas, C.R., Sarmiento, A.M., Pérez-Moreno, S.M., 2016. Pollutant flows from a phosphogypsum disposal area to an estuarine environment: an insight from geochemical signatures. Sci. Total Environ. 553, 42–51.
Pérez-López, R., Millán-Becerro, R., Basallote, M.D., Carrero, S., Parviainen, A., Freydier, R., Cánovas, C.R., 2023. Effects of estuarine water mixing on the mobility of trace elements in acid mine drainage leachates. Mar. Pollut. Bull. 187, 114491.
Rodier, J., Bazin, C., Broutin, J.P., Chambon, P., Champsaur, H., 1996. ET RODI, L. L'analyse de l'eau, 8e édition. Dunod (Éditeur), Paris, France.
Sainz, A., Grande, J.A., De la Torre, M.L., 2004. Characterisation of heavy metal discharge into the Ria of Huelva. Environ. Int. 30 (4), 557–566.
Smith, K.S., 1999. Metal sorption on mineral surfaces: an overview with examples relating to mineral deposits. In: Plumlee, G.S., Losdon, M.J. (Eds.), The Environmental Geochemistry of Mineral Deposits, Part A. Processes, Techniques, and Health Issues, Society of Economic Geologists, Rev. Econ. Geol. 6A, pp. 161–182.
Van Geen, A., Adkins, J.F., Boyle, E.A., Nelson, C.H., Palanques, A., 1997. A 120-yr record of widespread contamination from mining of the Iberian pyrite belt. Geology 25 (4), 291–294.
Yaciuk, P.A., Colombo, F., Lecomte, K.L., De Micco, G., Bohé, A.E., 2022. Cadmium sources, mobility, and natural attenuation in contrasting environments (carbonate-rich and carbonate-poor) in the Capillitas polymetallic mineral deposit. NW Argentina. Applied Geochemistry 136, 105152.
Zhou, J.L., Liu, Y.P., Abrahams, P.W., 2003. Trace metal behaviour in the Conwy estuary. North Wales. Chemosphere 51 (5), 429–440.